THE JOURNAL OF BIOLOGICAL CHEMISTRY VOL. 284, NO. 3, pp. 1732–1740, January 16, 2009

Lesion Bypass of N^2-Ethylguanine by Human DNA Polymerase ι*

Received for publication, September 19, 2008, and in revised form, October 31, 2008 Published, JBC Papers in Press, November 3, 2008, DOI 10.1074/jbc.M807296200

Matthew G. Pence[‡], Patrick Blans[§], Charles N. Zink[§], Thomas Hollis[‡], James C. Fishbein[§], and Fred W. Perrino[‡1]

From the [‡]Department of Biochemistry and Center for Structural Biology, Wake Forest University Health Sciences, Winston-Salem, North Carolina 27157 and the [§]Department of Chemistry and Biochemistry, University of Maryland, Baltimore County, Baltimore, Maryland 21250

Nucleotide incorporation and extension opposite N^2-ethyl-Gua by DNA polymerase ι was measured and structures of the DNA polymerase ι-N^2-ethyl-Gua complex with incoming nucleotides were solved. Efficiency and fidelity of DNA polymerase ι opposite N^2-ethyl-Gua was determined by steady state kinetic analysis with Mg^{2+} or Mn^{2+} as the activating metal. DNA polymerase ι incorporates dCMP opposite N^2-ethyl-Gua and unadducted Gua with similar efficiencies in the presence of Mg^{2+} and with greater efficiencies in the presence of Mn^{2+}. However, the fidelity of nucleotide incorporation by DNA polymerase ι opposite N^2-ethyl-Gua and Gua using Mn^{2+} is lower relative to that using Mg^{2+} indicating a metal-dependent effect. DNA polymerase ι extends from the N^2-ethyl-Gua:Cyt 3′ terminus more efficiently than from the Gua:Cyt base pair. Together these kinetic data indicate that the DNA polymerase ι catalyzed reaction is well suited for N^2-ethyl-Gua bypass. The structure of DNA polymerase ι with N^2-ethyl-Gua at the active site reveals the adducted base in the *syn* configuration when the correct incoming nucleotide is present. Positioning of the ethyl adduct into the major groove removes potential steric overlap between the adducted template base and the incoming dCTP. Comparing structures of DNA polymerase ι complexed with N^2-ethyl-Gua and Gua at the active site suggests movements in the DNA polymerase ι polymerase-associated domain to accommodate the adduct providing direct evidence that DNA polymerase ι efficiently replicates past a minor groove DNA adduct by positioning the adducted base in the *syn* configuration.

N^2-Ethylguanine (N^2-ethyl-Gua)[2] is an acetaldehyde-derived DNA adduct generated from the reduction of acetaldehyde with 2′-deoxyguanosine-3′-monophosphate (1). Humans are exposed to acetaldehyde from the environment and through the formation of acetaldehyde by the oxidation of ethanol (2). N^2-Ethyl-Gua has been detected in the DNA of both alcoholic and nonalcohol drinkers (2, 3). Ethanol is classified as a human carcinogen, and acetaldehyde is known to contribute to the formation of malignant tumors (4). The formation of N^2-ethyl-Gua during the reduction of acetaldehyde could cause ethanol-related cancers (5).

The ethyl moiety of N^2-ethyl-Gua is predicted to project into the minor groove of duplex DNA. The N^2-ethyl-Gua adduct is a strong block to DNA replication by replicative DNA polymerases *in vitro* and in cells (6, 7). Structures of bacteriophage DNA polymerase (pol) RB69, a homolog of human DNA pol α, indicate a possible mechanism of N^2-ethyl-Gua blocked DNA replication. The structures reveal a DNA-binding motif that contacts the DNA minor groove and functions as an important safeguard to replication fidelity (8). The blocking of replicative DNA pols by N^2-ethyl-Gua could arise when the ethyl group, protruding into the minor groove, disrupts protein:DNA contacts involved in the proposed "checking mechanism" (8). N^2-Ethyl-Gua also has a high mis-coding potential during DNA replication with the Klenow fragment of *Escherichia coli* DNA pol I (9). Mutations caused by N^2-ethyl-Gua range from single base deletions to transversions (10).

The Y family DNA polymerases η, ι, and κ replicate through adducted DNA templates (6, 11–13) and an open, more rigid active site contributes to lesion bypass (14). The multitude of Y family DNA pols suggests that a variety of mechanisms might be utilized by these polymerases during lesion bypass dependent upon the nature of the specific DNA adducts. Structural data indicate that DNA pol ι rotates unadducted template purines from the *anti* to *syn* conformation in ternary complexes and forms hydrogen bonds between the Hoogsteen edge of the template base and the Watson-Crick edge of the incoming nucleotide (15–17). Kinetic studies show that DNA pol ι has increased efficiency and fidelity during nucleotide insertion opposite template purines (11, 18–20). Similarly, rotation of the template base to the *syn* conformation is observed in the structure of DNA pol ι complexed with the 1,N^6-ethenodeoxyadenosine lesion, allowing correct nucleotide insertion but not subsequent extension opposite the adduct (21). Rotation of the purine base at the active site of DNA pol ι would allow for efficient bypass of DNA adducts at the N^2 of Gua by repositioning the adduct into the major groove and removing potential steric overlap between the lesion and incoming nucleotide. Thus, DNA pol ι could be involved in the bypass of the minor groove DNA adduct N^2-ethyl-Gua.

* This work was supported, in whole or in part, by National Institutes of Health Grants GM069962 (to F. W. P.) and CA52881 (to J. C. F.). This work was also supported by American Cancer Society Grant RSG-04-187-01-GMC (to T. H.). The costs of publication of this article were defrayed in part by the payment of page charges. This article must therefore be hereby marked "*advertisement*" in accordance with 18 U.S.C. Section 1734 solely to indicate this fact.

The atomic coordinates and structure factors (codes 3EPG and 3EPI) have been deposited in the Protein Data Bank, Research Collaboratory for Structural Bioinformatics, Rutgers University, New Brunswick, NJ (http://www.rcsb.org/).

[1] To whom correspondence should be addressed. Tel.: 336-716-4349; Fax: 336-716-7671; E-mail: fperrino@wfubmc.edu.

[2] The abbreviations used are: N^2-ethyl-Gua, N^2-ethylguanine; DNA pol ι, DNA polymerase ι; PAD, polymerase-associated domain; pol, polymerase; MES, 4-morpholineethanesulfonic acid.

The DNA polymerases utilize two divalent metal ions for activation of catalysis (22–24). The metals play a role in binding and positioning of the incoming nucleotide and in determining fidelity during catalysis (24, 25). The Mg^{2+} ion is often used as the activating metal for DNA polymerization studies *in vitro* (24). The Mn^{2+} ion also binds to and activates DNA polymerases but frequently results in decreased fidelity of the replicative DNA polymerases (26, 27). Recently, the Mn^{2+} ion has been shown to increase the efficiency and fidelity of nucleotide incorporation by DNA pol ι opposite a template Thy nucleotide (28).

The strong blocking effect of N^2-ethyl-Gua to the replicative DNA polymerases and its possible role in alcohol-related cancers have prompted our studies on bypass of N^2-ethyl-Gua by the Y family DNA pol ι. These data provide new insights into replication bypass of the ethanol-derived N^2-ethyl-Gua adduct with potential carcinogenic consequences. The structures of DNA pol ι complexed with N^2-ethyl-Gua containing DNA provide direct evidence for the initial *anti* position of the N^2-ethyl-Gua that is subsequently rotated into the *syn* position upon binding the correct Cyt nucleotide but not upon binding the incorrect Thy nucleotide. The N^2-ethyl moiety is easily accommodated in the major groove binding pocket of DNA pol ι by the specific repositioning of Lys^{309} located in a loop of the PAD domain. The Lys^{309} hydrogen bonding to the 5′ phosphate of the N^2-ethyl-Gua template base in the *anti* orientation repositions to accommodate the ethyl side chain. This repositioning of Lys^{309} defines the available space for accommodation of relatively small adducts such as the alkyl lesions at the N^2 position of Gua for efficient replication past these lesions by DNA pol ι. Furthermore, we show that when Mn^{2+} is the activating divalent metal, DNA pol ι bypass of N^2-ethyl-Gua occurs with increased efficiency but reduced fidelity compared with Mg^{2+}, demonstrating that Mn^{2+} could play an important role in modulating efficiency and fidelity of lesion bypass of minor groove purine adducts like N^2-ethyl-Gua by the Y family DNA polymerases. Consequences of Mn^{2+} as the activating metal and flexibility of the DNA pol ι PAD domain for efficient bypass of N^2-ethyl-Gua are discussed.

EXPERIMENTAL PROCEDURES

Oligonucleotides—N^2-Ethyl-Gua phosphoramidites and template oligonucleotides were prepared as described previously (6). Three DNA primer oligonucleotides, 5′-(6-FAM)-GCTCCGGAACCC-3′, 5′-(6-FAM)-GCTCCGGAACCCTT-3′, and 5′-(6-FAM)-GCTCCGGAACCCTTC-3′, were purchased from Operon Biotechnologies, Inc. (Huntsville, AL). For crystallization experiments, a self-annealing DNA oligonucleotide containing the N^2-ethyl-Gua adduct and a dideoxy CMP at the 3′ end, 5′-TCT*X*GGGTCCTAGGACCddC-3′ (where *X* = N^2-ethyl-Gua), was synthesized by Midland Certified Reagents (Midland, TX) using the supplied N^2-ethyl-Gua phosphoramidites. Synthesis was carried out using cyanoethyl phosphoramidite chemistry, and protecting groups were removed by hydrolysis with concentrated ammonium hydroxide (20). The oligo was purified by reverse phase high performance liquid chromatography (mass calculated = 5503.7, mass observed = 5504.9).

Expression and Purification of Human DNA Polymerase ι—The recombinant catalytic fragment of human DNA pol ι (amino acids 1–420) was made as an maltose-binding protein-DNA pol ι fusion protein with a PreScission Protease cleavage site seven residues from the DNA pol ι N-terminal methionine. The PreScission Protease recognition sequence and DNA pol ι coding sequence were verified by DNA sequencing. The plasmid constructs were transformed into *E. coli* BL21(DE3) Rosetta 2 cells (Novagen) for overexpression. Cells were grown to an A_{600} = 0.5 at 37 °C and quickly cooled on ice to 17 °C. After induction with 1 mM isopropyl β-D-thiogalactopyranoside, the cells were allowed to grow for 15 h at 17 °C. Cell extracts were prepared and the maltose-binding protein-DNA pol ι fusion protein was bound to an amylose resin in buffer containing 20 mM Tris-HCl (pH 7.5), 1 mM EDTA, and 200 mM NaCl. The fusion protein was cleaved overnight by on-column incubation with PreScission Protease at 4 °C. The recovered DNA pol ι was purified to homogeneity using phosphocellulose chromatography.

Assays—For primer extension assays the DNA primer (12-mer) was hybridized to the 32-mer DNA template and added to reactions containing 20 mM Tris-HCl (pH 7.5), 2 mM dithiothreitol, 100 μM dNTP, 10 nM DNA pol ι, and the amount of $MgCl_2$ or $MnCl_2$ indicated in the figure legends. Incubations were for 15 min at 37 °C and reactions were quenched with EtOH. Samples were dried and resuspended in 5 μl of a 95% formamide/dye solution. Extension products were separated on 23% urea-polyacrylamide gels, and imaged with a PhosphorImager (Molecular Dynamics) and quantified using ImageQuant software.

For the kinetic assays, the site-specific insertion procedure of Boosalis *et al.* (29) was used. DNA primers (14-mer for insertion and 15-mer for extension) were hybridized to the 32-mer DNA templates and added to reactions containing 20 mM Tris-HCl (pH 7.5), 2 mM dithiothreitol, 2 mM $MgCl_2$ or 0.075 mM $MnCl_2$, 50 nM primer-template, and 0.625 nM DNA pol ι (Mg^{2+}-activated reactions), or 0.2 nM DNA pol ι (Mn^{2+}-activated reactions). The amounts of DNA pol ι in reactions yielded ~20% extended product maximally. Incubations were for 10 min at 37 °C and reactions were processed as described above. All extended product bands were used to determine kinetic parameters (K_m and k_{cat} values) by non-linear regression using SigmaPlot 8.02 software (SPSS Science, Inc.). Relative insertion frequencies were calculated as $1/[(k_{cat}/K_{M,correct})/(k_{cat}/K_{M,incorrect})]$.

Crystallization of Human DNA Pol ι—The purified catalytic fragment of DNA pol ι was dialyzed into 20 mM $NaPO_4$ monobasic, 1 mM EDTA, 1 mM dithiothreitol, and 150 mM NaCl and concentrated to ~11 mg/ml. The DNA pol ι was mixed at a 1:1.2 molar ratio with the N^2-ethyl-Gua containing DNA oligonucleotide. To study ternary complexes, $MgCl_2$ and dCTP (or dTTP) were added to final concentrations of 10 and 20 mM, respectively. Crystals grew from solutions described by Nair *et al.* (16) containing 0.2–0.4 M $(NH_4)_2SO_4$, 12.5–15% PEG 5000 monomethyl ether, and 0.1 M MES (pH 6.5). Crystal trays were kept at 4 °C and diffraction quality crystals appeared in 1–3 days. The crystals belonged to space group $P6_522$ and had cell dimensions of $a = b = 98.53$ Å, $c = 202.35$ Å for dCTP con-

taining crystals, and $a = b = 98.64$ Å, $c = 202.23$ Å for dTTP containing crystals, and $\alpha = \beta = 90°$, $\gamma = 120°$. For data collection crystals were step soaked for 5 min in mother liquor solutions containing 0–25% glycerol and flash frozen in liquid nitrogen.

Structure Determination and Refinement—X-ray diffraction data were collected using CuKα radiation from an in-house MicroMax 007 generator on a Saturn 92 CCD detector (Rigaku). The data were indexed, integrated, and scaled using d*TREX (30), and phases were calculated using molecular replacement. Molecular replacement with Phaser (31) generated a unique solution using DNA pol ι (Protein Data Bank code 2ALZ) minus DNA as a search model. Electron density maps calculated to 2.5 Å (dCTP) and 2.9 Å (dTTP) showed clear density around the N^2-ethyl-Gua lesion. The dCTP ternary structure showed good electron density for the incoming nucleotide. Electron density for incoming dTTP could not be seen except for the γ phosphate, which was included in the model. Models were built in COOT (32) and refined in REFMAC5 using translesion systhesis refinement (33, 34). The refined model converged to an $R_{cryst} = 23.2\%$ and $R_{free} = 28.6\%$ for the dCTP-containing complex and $R_{cryst} = 23.6\%$ and $R_{free} = 28.2\%$ for the dTTP-containing complex. Ramachandran plots for the refined models show good stereochemistry, with 87.4 (dCTP-containing) and 88.6% (dTTP-containing) of residues in the favored regions and 0.0 (dCTP-containing) and 0.0% (dTTP-containing) in the disallowed regions. Figures were prepared using PyMol (35).

RESULTS

Primer Extension Reactions—DNA polymerase ι catalyzes bypass of the N^2-ethyl-Gua adduct using Mg^{2+} or Mn^{2+} as the activating divalent metal ion. DNA polymerases can utilize various activating divalent metals (22–25, 28) and recent evidence indicates that both Mg^{2+} and Mn^{2+} are potent activators of DNA pol ι with perhaps Mn^{2+} being the preferred metal ion for activation (28). The DNA pol ι catalyzed bypass of N^2-ethyl-Gua was tested using Mg^{2+} or Mn^{2+} as the activating metal (Fig. 1). A 12-mer DNA primer was annealed to 32-mer DNA templates with the primer 3′ terminus positioned three nucleotides from the target N^2-ethyl-Gua or Gua (Fig. 1*A*). Upon incubation of the primer-template with DNA pol ι the 12-mer primer is extended to generate products 13 to 19 nucleotides in length and no full-length 25-nucleotide products are observed (Fig. 1, *B* and *C*). These data are consistent with the previously described poor primer extension properties of DNA pol ι, which exhibits especially low efficiency when copying template pyrimidines like those positioned 5′ to the target site in this template design (18, 36, 37). Primer extension reactions performed in the presence of increased concentrations of $MgCl_2$ (Fig. 1*B*) or $MnCl_2$ (Fig. 1*C*) show that DNA pol ι exhibits considerable sensitivity to the divalent ion concentration as indicated by the observed products. The maximum level of primer extension was detected using either DNA template at 2 mM $MgCl_2$ (Fig. 1*B*) and 0.075 mM $MnCl_2$ (Fig. 1*C*). Higher concentrations of $MgCl_2$ and $MnCl_2$ reduce DNA pol ι-catalyzed extension (Fig. 1, *B* and *C*, see also Ref. 28). These data indicate that DNA pol ι-catalyzed primer extension using the N^2-ethyl-Gua and Gua DNA templates is similar and that the maximum extension is achieved at a ~26-fold lower concentration of Mn^{2+} ion compared with Mg^{2+}.

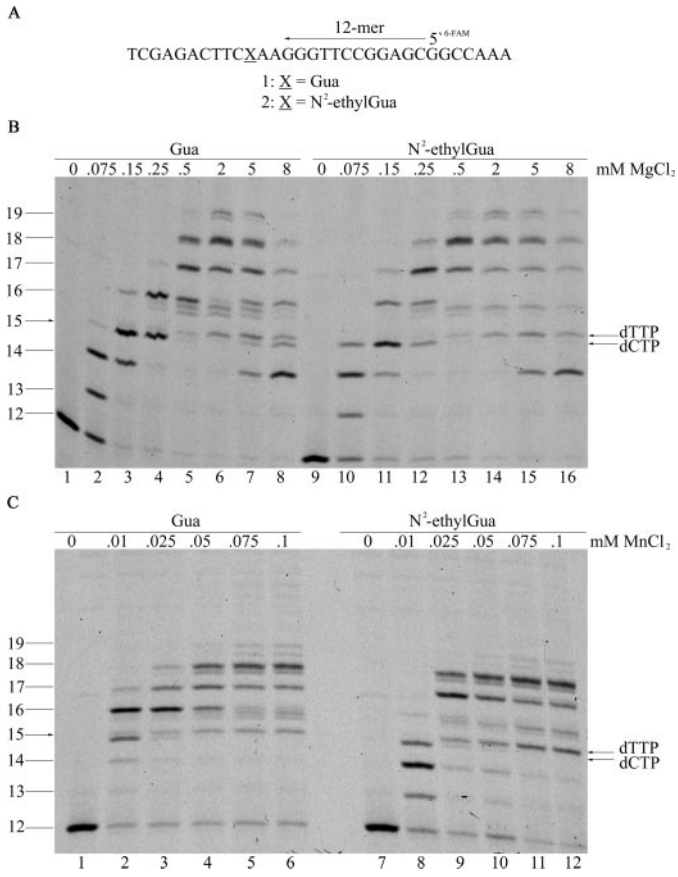

FIGURE 1. **Extension opposite N^2-ethyl-Gua or Gua by DNA Pol ι in the presence of $MgCl_2$ or $MnCl_2$.** Primer extension assays were carried out as described under "Experimental Procedures." The annealed primer (12-mer) and templates containing either N^2-ethyl-Gua or Gua (*A*) were incubated with 10 nM DNA pol ι and increasing concentrations of $MgCl_2$ (*B*) or $MnCl_2$ (*C*). Maximal primer extension was observed at 2 mM $MgCl_2$ and 0.075 mM $MnCl_2$. In single nucleotide extension reactions with only dTTP or dCTP using the 14-mer primer, the 15-mer product of dTMP insertion migrates to the position of the upper band and the 15-mer product of dCMP insertion migrates to the position of the lower band (data not shown).

Insertion of the correct dCMP and incorrect dTMP opposite Gua and N^2-ethyl-Gua by DNA pol ι is detected using either Mg^{2+} or Mn^{2+} as the activating metal. The 15-nucleotide products are detected as a doublet band corresponding to the correct incorporation of two dTMP nucleotides opposite the template adenines to generate the 14-nucleotide products and subsequent incorporation of dCMP or dTMP opposite the target Gua and N^2-ethyl-Gua by DNA pol ι (Fig. 1, *B* and *C*). The product band corresponding to dCMP insertion opposite template Gua, but not template N^2-ethyl-Gua, was detected at the higher $MgCl_2$ concentrations tested suggesting that DNA pol ι extends the N^2-ethyl-Gua:Cyt base pair more efficiently than the normal Gua:Cyt base pair when Mg^{2+} is the activating metal ion (Fig. 1*B*, compare *lanes 7* and *8* to *15* and *16*). The presence of the 15-nucleotide product band corresponding to insertion of dTMP opposite the target Gua and N^2-ethyl-Gua in the most active primer extension reactions indicates that DNA pol ι extends more efficiently from the correctly base paired

TABLE 1

Nucleotide insertion opposite Gua and N^2-ethyl-Gua by DNA pol ι

K_m and k_{cat} values were determined by quantifying gel band intensities using ImageQuant, and non-linear regression analysis of product *versus* [dNTP] curves, using SigmaPlot 8.0.2.

Metal ion	dNTP	K_m	k_{cat}	k_{cat}/K_m	Relative insertion frequency[a]
		μM	min^{-1}	$min^{-1}\ \mu M^{-1}$	
At template N^2-ethyl-Gua					
0.075 mM Mn^{2+}					
	Cyt	0.10 ± 0.012	425 ± 15	4.3×10^3	1
	Thy	0.030 ± 0.014	225 ± 25	7.5×10^3	1/0.6
2 mM Mg^{2+}					
	Cyt	36 ± 3	74 ± 12	2.1×10^0	1
	Thy	650 ± 180	115 ± 18	1.8×10^{-1}	1/12
At template Gua					
0.075 mM Mn^{2+}					
	Cyt	0.15 ± 0.020	700 ± 40	4.7×10^3	1
	Thy	0.085 ± 0.020	200 ± 15	2.4×10^3	1/2
2 mM Mg^{2+}					
	Cyt	49 ± 4	112 ± 18	2.3×10^0	1
	Thy	220 ± 60	50 ± 6	2.3×10^{-1}	1/10

[a] Relative insertion frequency is calculated as 1/([k_{cat}/K_m, correct]/[k_{cat}/K_m, incorrect]).

TABLE 2

Extension from Gua:Cyt, Gua:Thy, and N^2-ethyl-Gua:Cyt, N^2-ethyl-Gua:Thy base pairs by DNA pol ι

K_m and k_{cat} values were determined by quantifying gel band intensities using ImageQuant, and non-linear regression analysis of product *versus* [dNTP] curves, using SigmaPlot 8.0.2.

Metal ion	Base pair	K_m	k_{cat}	k_{cat}/K_m	Relative extension frequency[a]
		μM	min^{-1}	$min^{-1}\ \mu M^{-1}$	
At template N^2-ethyl-Gua					
0.075 mM Mn^{2+}					
	N^2-Et-Gua:Cyt[b]	0.10 ± 0.012	210 ± 7	2.1×10^3	1
	N^2-Et-Gua:Thy	0.30 ± 0.027	1.0 ± 0.02	3.3×10^0	1/640
2 mM Mg^{2+}					
	N^2-Et-Gua:Cyt	40 ± 1	90 ± 4	2.3×10^0	1
	N^2-Et-Gua:Thy	160 ± 40	0.31 ± 0.03	1.9×10^{-3}	1/1180
At template Gua					
0.075 mM Mn^{2+}					
	Gua:Cyt	0.25 ± 0.045	220 ± 10	8.8×10^2	1
	Gua:Thy	1.1 ± 0.09	1.3 ± 0.04	1.2×10^0	1/730
2 mM Mg^{2+}					
	Gua:Cyt	200 ± 30	110 ± 8	5.5×10^{-1}	1
	Gua:Thy	170 ± 30	0.18 ± 0.013	1.1×10^{-3}	1/500

[a] Relative extension frequency is calculated as 1/([k_{cat}/K_m, correct]/[k_{cat}/K_m, incorrect]).
[b] Et, ethyl.

Gua:Cyt and N^2-ethyl-Gua:Cyt 3′ termini relative to extension from the mispaired Gua:Thy and N^2-ethyl-Gua:Thy termini (Fig. 1, *B* and *C*). The triplet band corresponding to the 16-nucleotide position indicates additional heterogeneity in the oligonucleotide product 3′ terminal sequence likely resulting from the low level of nucleotide discrimination by DNA pol ι during nucleotide incorporation opposite template cytosines (37).

Efficiency and Fidelity of N^2-Ethyl-Gua Bypass by DNA Pol ι—A steady state kinetic assay was used to more precisely quantify the efficiency and fidelity of DNA pol ι bypass of N^2-ethyl-Gua compared with Gua in the presence of $MgCl_2$ or $MnCl_2$. Nucleotide insertion reactions were performed in the presence of increased concentrations of dCTP or dTTP using primed templates with the 3′ terminus positioned one nucleotide before the N^2-ethyl-Gua or Gua. Extension reactions were performed in the presence of increased concentrations of the next correct nucleotide dGTP using primed templates with the 3′ Cyt or Thy positioned opposite the N^2-ethyl-Gua or Gua. These data were quantified and the summary presented in Tables 1 and 2.

The DNA pol ι inserts the correct dCMP or incorrect dTMP nucleotide at high efficiency in the presence of Mn^{2+}. The efficiency (k_{cat}/K_m) of dCMP insertion by DNA pol ι opposite N^2-ethyl-Gua in the presence of Mn^{2+} is ~2,000-fold higher than that measured in the presence of Mg^{2+}, and there is a similar high efficiency for dCMP insertion opposite Gua in the presence of Mn^{2+} compared with Mg^{2+}. The dramatically higher efficiency measured in the presence of Mn^{2+} can be attributed to a ~340-fold lower K_m value and a ~6-fold higher k_{cat} value during correct nucleotide incorporation for both DNA templates (Table 1). The efficiency of incorrect dTMP insertion by DNA pol ι opposite N^2-ethyl-Gua in the presence of Mn^{2+} is ~42,000-fold higher than that in the presence of Mg^{2+} and ~10,000-fold higher opposite Gua using Mn^{2+} compared with Mg^{2+}. Similar to that observed during correct nucleotide insertion, the higher efficiency for incorrect nucleotide insertion measured in the presence of Mn^{2+} is mostly attributable to a much lower K_m value for the nucleotide using both DNA templates. These data suggest that DNA pol ι binds correct and incorrect incoming nucleotides with greater affinity and catalyzes nucleotide addition more rapidly in the Mn^{2+}-activated reaction compared with the Mg^{2+}-activated reaction.

The DNA pol ι exhibits higher fidelity of nucleotide insertion opposite N^2-ethyl-Gua and Gua when activated with Mg^{2+} compared with Mn^{2+}. Relative insertion frequencies calculated

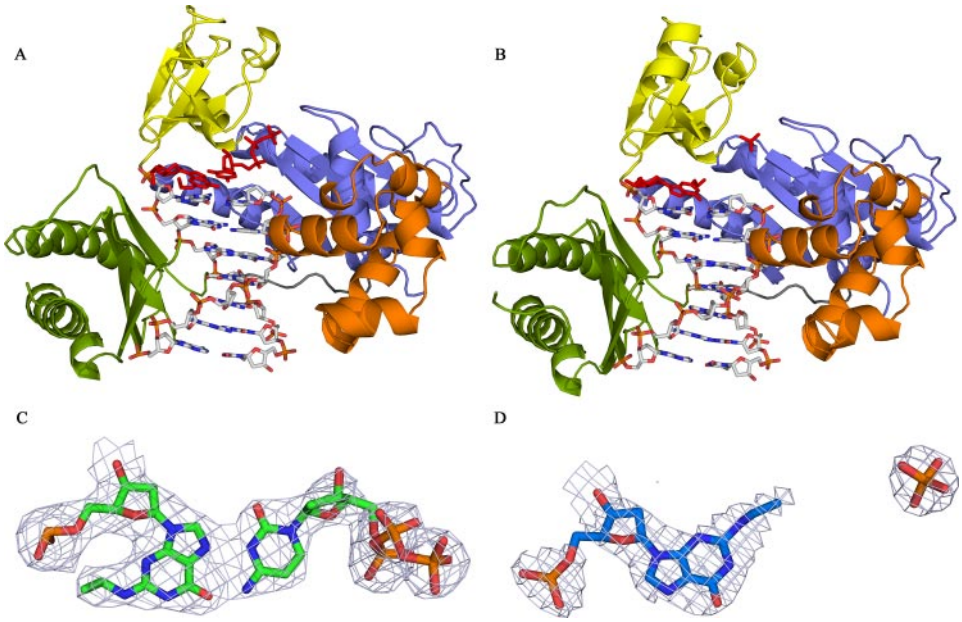

FIGURE 2. **The structures of DNA pol ι·N^2-ethyl-Gua Complexes with incoming dCTP or dTTP.** *A*, the structure of DNA pol ι containing N^2-ethyl-Gua and incoming dCTP shows the N^2-ethyl-Gua base rotated into the *syn* configuration. *B*, the structure of DNA pol ι containing N^2-ethyl-Gua and incoming dTTP shows the N^2-ethyl-Gua base in the *anti* configuration and the N^2-adduct protruding into the minor groove. *C*, electron density around the N^2-ethyl adduct and incoming dCTP. *D*, electron density around the N^2-ethyl adduct and the γ phosphate of the incoming dTTP.

for incorrect dTMP opposite N^2-ethyl-Gua and Gua in the presence of Mg^{2+} are lower compared with those measured using Mn^{2+} indicating an increased level of fidelity in the presence of Mg^{2+}. Of particular note is the 20-fold higher level of nucleotide discrimination observed opposite N^2-ethyl-Gua in the presence of Mg^{2+} compared with Mn^{2+} indicating a metal-dependent increase in the level of nucleotide discrimination opposite the adducted N^2-ethyl-Gua by DNA pol ι. These data are similar to previous observations that Mn^{2+} causes a decreased fidelity in the replicative DNA polymerases (26, 27, 38, 39).

The DNA pol ι extends 3′ termini positioned opposite the N^2-ethyl-Gua with higher efficiency in the presence of Mn^{2+} compared with Mg^{2+}. The k_{cat}/K_m values for extension from the N^2-ethyl-Gua:Cyt and Gua:Cyt base pairs indicate a ~1300-fold higher extension efficiency in the presence of Mn^{2+} compared with Mg^{2+} (Table 2). The increased efficiency of extension using Mn^{2+} with either the adducted or unadducted DNA template is attributable to a ~600-fold lower K_m value for dGMP incorporation and a ~2.2-fold higher k_{cat} value (Table 2). Extension from the mispaired N^2-ethyl-Gua:Thy base pair and from the Gua:Thy base pair is ~1400-fold more efficient in the presence of Mn^{2+} compared with Mg^{2+} (Table 2). Interestingly, the efficiency of extension from a 3′ terminus positioned opposite the N^2-ethyl-Gua is ~3-fold higher than extension from a 3′ terminus opposite Gua using either Mg^{2+} or Mn^{2+} (Table 2).

The relative extension frequencies indicate that DNA pol ι distinguishes the correctly paired N^2-ethyl-Gua:Cyt from the incorrectly paired N^2-ethyl-Gua:Thy better in the presence of Mg^{2+} compared with Mn^{2+}. The calculated relative extension frequency from 3′ termini opposite N^2-ethyl-Gua in the presence of Mg^{2+} is ~2-fold lower than that determined in the presence of Mn^{2+} (Table 2). The relative extension frequencies from 3′ termini positioned opposite the unadducted Gua using Mg^{2+} is similar to that using Mn^{2+} indicating that this apparent metal-dependent effect is not detected during extension from 3′ termini positioned opposite Gua.

The Structure of DNA Pol ι with N^2-Ethyl-Gua in the Active Site—The DNA pol ι bypasses N^2-ethyl-Gua by rotating the adducted Gua base into the *syn* conformation. The crystal structure of N^2-ethyl-Gua positioned in the active site of DNA pol ι was solved revealing the N^2-ethyl-Gua in the *syn* conformation when the correct incoming dCTP nucleotide was present and in the *anti* configuration in the presence of the incorrect dTTP nucleotide (Fig. 2, Table 3). These data provide direct structural evidence that DNA pol ι bypasses the N^2-ethyl-Gua adduct by rotating the adducted Gua to position the N^2-ethyl adduct into the major groove. The crystal structures of DNA pol ι·N^2-ethyl-Gua ternary complexes in the presence of dCTP (Fig. 2*A*) or dTTP (Fig. 2*B*) were solved to 2.5- and 2.9-Å resolution, respectively. The data show clear electron density for the ethyl adduct in both complexes (Fig. 2, *C* and *D*) as well as clear electron density for incoming dCTP (Fig. 2*C*). Data collected from crystals grown in the presence of dTTP lack electron density for the incoming nucleotide except around the γ phosphate (Fig. 2*D*). Electron density around the N^2-ethyl-Gua adduct in the presence of incorrect dTTP shows that the template adducted base is in the *anti* configuration. Thus, our data show that N^2-ethyl-Gua is in the *syn* configuration when paired with the correct dCTP and in the *anti* configuration when no paired nucleotide is detected. These data parallel the results of Nair *et al.* (17) who describe the incoming nucleotide as imposing a *syn* conformation on unadducted templates and extends the relevance of their observation to the N^2-ethyl-Gua adducted DNA template.

The rotation of N^2-ethyl-Gua into the *syn* conformation and consequent positioning of the N^2-ethyl moiety into the major groove disrupts contact between a DNA pol ι residue in the PAD domain and the DNA backbone. The two DNA pol ι·N^2-ethyl-Gua complexes generated here were superimposed with the two DNA pol ι·Gua complexes determined by Nair *et al.* (PDB accession codes 2ALZ and 2FLP (16, 17)) to compare the structures (Fig. 3). As expected, the overall structures are very similar and align with root mean square deviation values of 0.499 Å (structures of DNA pol ι with N^2-ethyl-Gua or Gua (2ALZ) in the *syn* configuration) and 0.466 Å (structures of N^2-ethyl-Gua and Gua (2FLP) in the *anti* configuration). These analyses indicate that residues 306–311, which constitute a

TABLE 3
Collection and refinement statistics

Data collection	DNA pol ι:N^2-ethyl-Gua with dCTP	DNA pol ι:N^2-ethyl-Gua with dTTP
Resolution (Å)[a]	2.2 (2.28-2.2)	2.9 (3.0-2.9)
No. of measured reflections	529,938	368,190
No. of unique reflections	19,625	13,417
Completeness (%)	98.9 (90.6)	100 (100)
Redundancy	17.7 (11.7)	27.4 (26.3)
R_{merge} (%)[b]	12.2 (40)	14.4 (32.3)
Mean I/σ	13 (5.1)	11.8 (4.0)
Refinement		
Resolution range (Å)	15–2.5	15–2.9
Reflections	19,625	12,753
R_{cryst} (%)[c]	23.2	23.8
R_{free} (%)[d]	28.6	28.2
Root mean square deviation bond lengths (Å)	0.019	0.010
Root mean square deviation bond angles (°)	1.8	1.5
Mean *B*-factor (Å^2)		
Protein	34.5	14.9
DNA	35.8	15.0
H_2O	32.9	13.9

[a] Values for outermost shells are given in parentheses.
[b] $R_{merge} = \Sigma|I - \langle I\rangle|/\Sigma I$, where I is the integrated intensity of a given reflection.
[c] $R_{cryst} = \Sigma||F_{observed}| - |F_{calculated}||/\Sigma|F_{observed}|$.
[d] R_{free} was calculated using 5% random data omitted from the refinement.

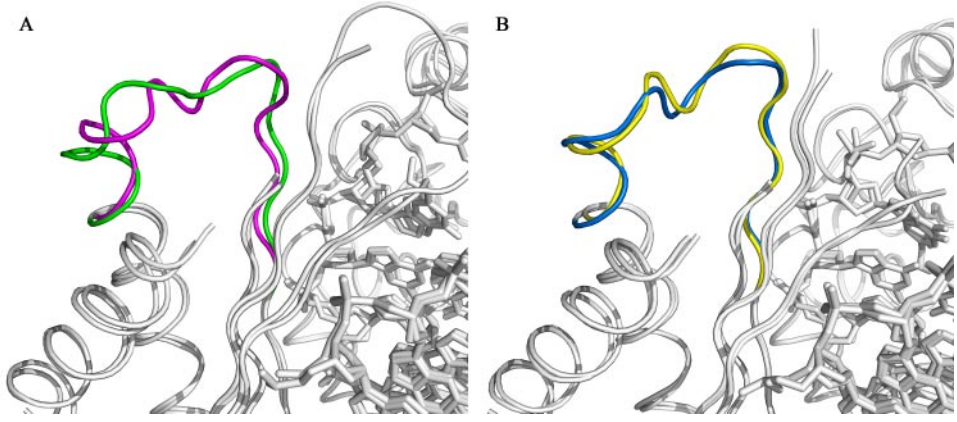

FIGURE 3. **Superposition of DNA pol ι complexes with *anti* and *syn* configurations of N^2-ethyl-Gua and Gua.** *A*, comparisons of the PAD domain in DNA pol ι with N^2-ethyl-Gua (*green*) or Gua (PDB code 2ALZ, *magenta*) rotated into the *syn* configuration demonstrate the change in position of the backbone atoms of the PAD loop. *B*, the repositioning of the loop is not observed when comparing structures of DNA pol ι with N^2-ethyl-Gua (*blue*) or Gua (PDB code 2FLP, *yellow*) rotated into the *anti* configuration.

loop in the PAD domain, move to accommodate the ethyl adduct when the N^2-ethyl-Gua is in the *syn* conformation in the active site. Detailed views of the DNA pol ι active sites in complex with N^2-ethyl-Gua or Gua are shown in Fig. 4. The presence of the ethyl group at the N^2 position of the N^2-ethyl-Gua, coupled with rotation to the *syn* conformation, results in a ~9 Å shift in the position of the Lys^{309} side chain as indicated by the different positions of Lys^{309} in the presence of *syn* N^2-ethyl-Gua compared with *syn* Gua (Fig. 4*A*). This repositioning of Lys^{309} is not observed when the N^2-ethyl-Gua or Gua base is in the *anti* conformation (Fig. 4*B*). Thus, the Lys^{309} side chain hydrogen bonds with the 5′ phosphate of the unadducted Gua in the *anti* or *syn* configuration and with the N^2-ethyl-Gua in the *anti* but not the *syn* configuration.

DISCUSSION

The Y family DNA polymerases bypass adducted DNA that would otherwise impede the completion of genomic replication by the replicative DNA polymerases. The Y family DNA polymerase responsible for translesion synthesis is reflected in the structural and catalytic properties of the DNA polymerase and the specific DNA lesion (14). Human DNA pol ι is unique among the DNA polymerases in synthesizing DNA using Hoogsteen base pairing rather than conventional Watson-Crick base pairing (15–17, 19, 21, 40). This DNA polymerase catalytic feature is particularly relevant to the replication of DNA adducts positioned at the exocyclic N^2 of Gua (6, 11, 20, 41–43). Our studies show that DNA pol ι inserts the correct dCTP opposite the N^2-ethyl-Gua adduct with the same efficiency as opposite Gua. These findings are consistent with previous results demonstrating DNA pol ι catalyzed incorporation opposite N^2-isopropyl-Gua and the N^2-adducts γ-HOPdGua and reduced γ-HOPdGua (20, 41, 42). Furthermore, our data indicate that DNA pol ι extends from the N^2-ethyl-Gua:Cyt 3′ terminus with higher efficiency compared with the Gua:Cyt 3′ terminus supporting previous findings from Choi and Guengerich (11). Together these data indicate that DNA pol ι bypasses N^2-ethyl-Gua by incorporation of the correct dCTP followed by increased extension efficiency from the N^2-ethyl-Gua:Cyt 3′ terminus. Thus, there is accumulating evidence that DNA pol ι exhibits increased extension efficiencies from adducted 3′ termini as has also been shown from N^2-methyl- and N^2-isobutyl-Gua adducts and from the reduced γ-HOPdGua (13, 42).

Our structural data provide evidence that DNA pol ι utilizes a Hoogsteen base pairing mechanism for efficient nucleotide incorporation during bypass of N^2-ethyl-Gua. The structural analysis shows that N^2-ethyl-Gua adopts a *syn* configuration in the active site of DNA pol ι in the presence of incoming dCTP. Rotation of template purines to the *syn* configuration has been

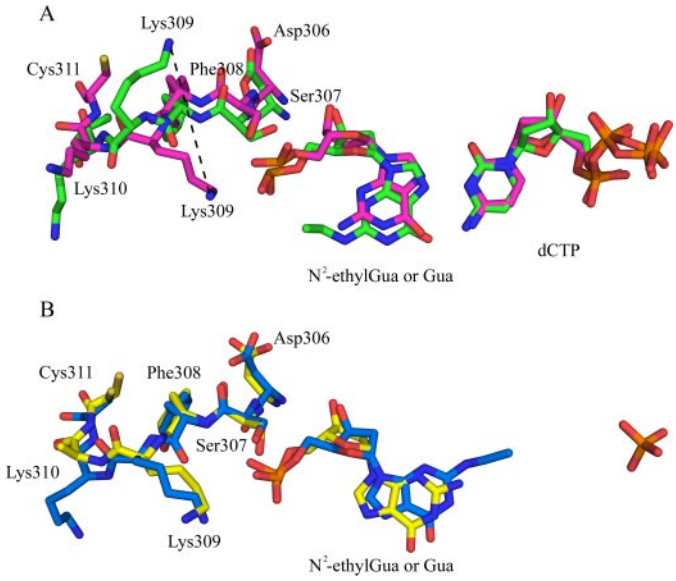

FIGURE 4. **Repositioning of Lys^{309} in the structure of DNA pol ι with N^2-ethyl-Gua in the *syn* configuration.** *A*, the Lys^{309} side chain in DNA pol ι in complex with N^2-ethyl-Gua (*green*) in the *syn* configuration shifts ~9 Å relative to the position of Lys^{309} in DNA pol ι complexed with *syn* Gua (PDB code 2ALZ, *magenta*). *B*, with N^2-ethyl-Gua in the *anti* conformation (*blue*) Lys^{309} remains in a similar position relative to the Lys^{309} in the DNA pol ι·Gua complex (PDB code 2FLP, *yellow*).

shown in structures of DNA pol ι complexed with template Gua or Ade, as well as 1,N^6-etheno-Ade (15–17, 21). These structural data support Hoogsteen base pairing as the mechanism utilized by DNA pol ι when incorporating nucleotides opposite adducted or unadducted purines. The ability of DNA pol ι to rotate Gua into the *syn* configuration allows bypass of the minor groove adduct N^2-ethyl-Gua. Rotation of the template base repositions the N^2-ethyl-Gua adduct into the major groove where there is less steric overlap between the lesion and incoming nucleotide and the residues at the active site. This unique ability of DNA pol ι to utilize Hoogsteen base pairing for efficient nucleotide incorporation opposite adducted template purines makes it a likely candidate DNA polymerase for bypass of minor groove adducts at the N^2 of Gua or adducts that disrupt normal Watson-Crick base pairing during DNA replication.

The DNA pol ι is not the only Y family DNA polymerase, however, able to efficiently bypass N^2-ethyl-Gua. Kinetic analyses using human DNA pols η and κ have shown that these DNA polymerases will efficiently bypass N^2-ethyl-Gua (6, 11). Structures of yeast DNA pol η and human DNA pol κ in complex with DNA show that the template base is in the *anti* configuration during nucleotide incorporation (44, 45). These kinetic and structural data suggest that DNA pols η and κ utilize a Watson-Crick base pairing mechanism during bypass of N^2-ethyl-Gua. A normal Watson-Crick base pair, however, cannot form between N^2-ethyl-Gua and incoming dCTP because of steric clash with the ethyl moiety and the O^2 atom of Cyt. It is possible that a wobble base pair with hydrogen bonds between the N^1 and O^6 of N^2-ethyl-Gua and the O^2 and N^3 of the incoming dCTP could form that would avoid steric overlap with the N^2-ethyl adduct during dCTP incorporation. A comparison of the Y family DNA polymerase structures in complex

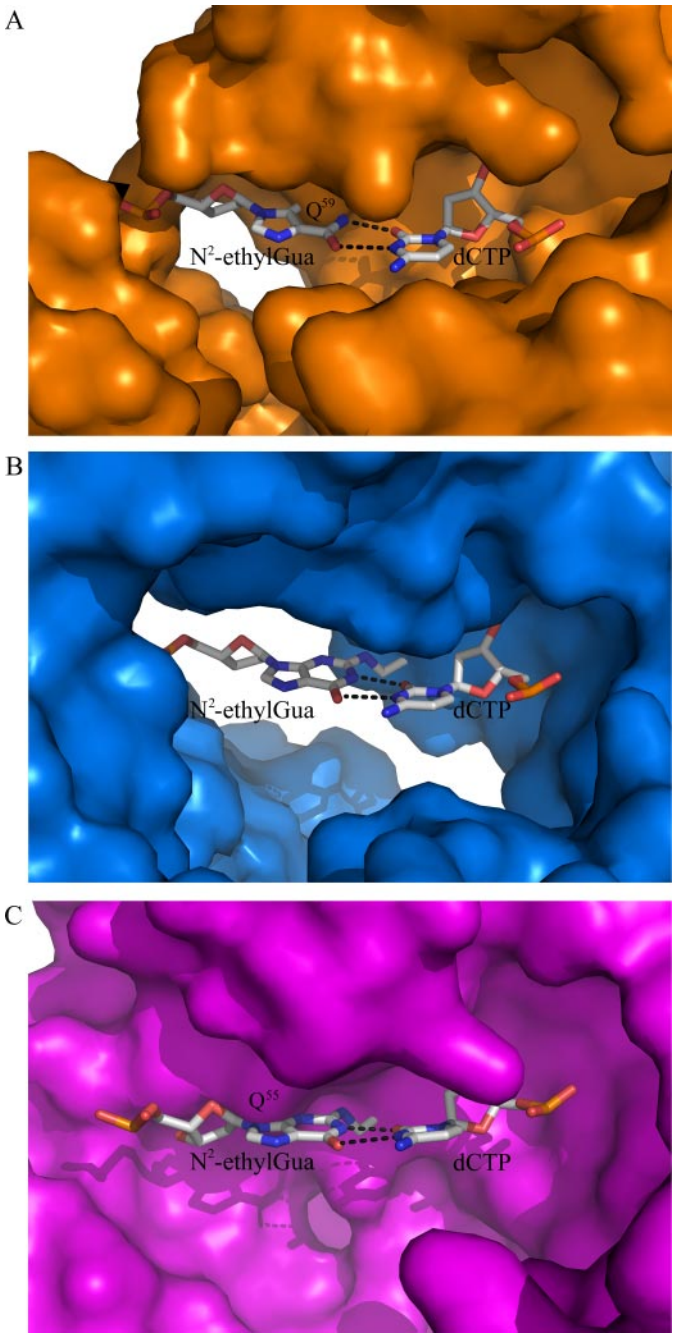

FIGURE 5. **A N^2-ethyl-Gua:Cyt wobble base in the active site of Y family DNA polymerases ι, κ, and η.** *A*, Gln^{59} in DNA pol ι tightly coordinates the template base and sterically clashes with N^2-ethyl-Gua when forming a wobble base pair with the incoming dCTP. *B*, DNA pol κ lacks a corresponding residue to Gln^{59} and accommodates the wobble base pair geometry. *C*, yeast DNA pol η has a Gln^{55} that corresponds to Gln^{59} in DNA pol ι but the more open active site accommodates the N^2-ethyl-Gua:Cyt wobble base pair.

with DNA shows that yeast DNA pol η (PDB 2R8J) and human DNA pol κ (PDB 2OH2) are able to accommodate wobble base pair geometry in their active sites, but human DNA pol ι is not (Fig. 5). The DNA pol ι active site more tightly coordinates the template base compared with DNA pols η and κ. Nair *et al.* (16, 17) have pointed out that this tight coordination, which shortens the C1′-C1′ distance between the sugars of the template nucleotide and incoming dNTP, forces the rotation of the template base into the *syn* conformation. In the active site of DNA

pol ι, Gln^{59} lies adjacent to the N^3 of N^2-ethyl-Gua stabilizing the alignment of the template base and incoming dCTP. Modeling an N^2-ethyl-Gua:Cyt wobble base pair into the active site of DNA pol ι reveals a ~20° rotation of the ethyl adduct toward Gln^{59} causing steric overlap between the lesion and Gln^{59} (Fig. 5*A*). The active site of DNA pol κ lacks a corresponding residue to Gln^{59} leaving the DNA minor groove free of protein contacts and able to accommodate the N^2-ethyl-Gua:Cyt wobble base pair (Fig. 5*B*). In yeast DNA pol η, Gln^{55} structurally aligns with the Gln^{59} residue of DNA pol ι but does not coordinate the template base as tightly. The DNA pol η active site is able to accommodate the N^2-ethyl-Gua:Cyt wobble base pair (Fig. 5*C*). These observations demonstrate how different Y family DNA polymerases could facilitate bypass of the N^2-ethyl-Gua adduct with or without rotation of the adducted base into the *syn* configuration.

The rotation of adducted purines from the *anti* to *syn* configuration is necessary but not always sufficient for bypass of minor groove adducts by DNA pol ι. The structural data show that DNA pol ι bypasses N^2-ethyl-Gua by a rotation of the adducted base and a repositioning of the lesion into the major groove. The ethyl moiety is accommodated in the major groove by changes in the positions of residues in a loop of the DNA pol ι PAD domain. Specifically, the potential for Lys^{309} to hydrogen bond with the DNA backbone is disrupted. The flexibility of the PAD domain allows accommodation of the ethyl moiety of N^2-ethyl-Gua, but may not accommodate adducts as large or larger than N^2-methyl(2-naphthyl)-Gua. Steady state kinetic data indicate that the efficiency of DNA pol ι during bypass of N^2-alkyl-Gua adducts is decreased at both the incorporation and extension steps when adduct size is increased (11). Assuming the adducted base is rotated into the *syn* configuration it is possible that the mobility of the PAD domain would limit the ability of DNA pol ι to accommodate larger adducts. Large DNA adducts could disrupt additional contacts between DNA pol ι and the major groove. These observations may explain the lower efficiency of DNA pol ι incorporation and extension measured during bypass of HNE-dGua or N^2-Naph-Gua, N^2-Anth-Gua, and N^2-BP-Gua adducts (11, 43).

Steady state kinetic experiments comparing the efficiency of DNA pol ι in the presence of Mg^{2+} or Mn^{2+} reveal that nucleotide insertion and extension catalyzed by DNA pol ι is dramatically activated at low Mn^{2+} concentrations. Our data show that maximal activation of DNA pol ι opposite Gua or N^2-ethyl-Gua is achieved at concentrations of 0.075 mM Mn^{2+} and higher, similar to what is observed when DNA pol ι copies unadducted DNA templates (28). Furthermore, in the simultaneous presence of Mg^{2+} and Mn^{2+} the activity of DNA pol ι during correct nucleotide insertion is intermediate of that observed in the presence of each metal individually and it has been suggested that DNA pol ι might preferentially use Mn^{2+} even in the presence of excess Mg^{2+} (28). The effects of Mn^{2+} on the fidelity of DNA pol ι vary between increased fidelity opposite template Thy to decreased fidelity opposite other unadducted and adducted DNA templates. Our data demonstrate a metal dependent increase in nucleotide discrimination opposite N^2-ethyl-Gua in the presence of Mg^{2+}. Thus, these observations suggest that the preferential use of Mn^{2+} as an activating metal might reduce the fidelity of lesion bypass by DNA pol ι in exchange for increased catalytic efficiency.

The concentration range required for maximum activity of DNA pol ι using Mn^{2+} is broader than that relative to Mg^{2+} where maximal activity is observed over a more narrow range of metal ion concentrations. DNA pol ι reaches a maximum activity at 2 mM Mg^{2+}, which decreases at higher Mg^{2+} ion concentrations. Current estimates indicate that total Mg^{2+} concentration in the cell ranges between 14 and 20 mM and free Mg^{2+} in the cytosol between 0.5 and 0.7 mM (46). The nucleus, mitochondrion, and endoplasmic reticulum are important cellular compartments for Mg^{2+} accumulation and Mg^{2+} levels are maintained within these cellular compartments by a sensitive regulatory system (46). It is possible that the level of Mg^{2+} maintained in the nucleus is at an optimal range for the highest activity of DNA pol ι, however, the narrow range of Mg^{2+} concentrations that result in maximal DNA pol ι activation would limit the efficiency of DNA pol ι catalyzed polymerization. The concentration of Mn^{2+} in the cell is much lower than Mg^{2+} and is thought to be around 10 μM (47). Interestingly, there have been several recently identified Mn^{2+} transporters from both eukaryotes and prokaryotes that are capable of transporting Mn^{2+} into the cell to bring the concentration to ≥300 μM. This influx of Mn^{2+} is in response to increased levels of reactive oxygen species (48). Thus, the broad range of Mn^{2+} concentrations that allow maximal DNA pol ι activity are present in the cell under damaging conditions where the higher efficiency of DNA pol ι opposite DNA lesions would be beneficial. DNA pol ι utilizes low levels of Mn^{2+} to achieve increased activity during bypass of other DNA adducts besides N^2-ethyl-Gua, including a thymine-thymine dimer, an abasic site, a (6-4)TT photoproduct, and a benzo[*a*]pyrene diol epoxide-deoxy adenine lesion (28). Importantly, we have shown that other Y family DNA polymerases, including DNA pol κ, also have increased activation in the presence of low concentrations of Mn^{2+}.[3] Thus, Mn^{2+} activation of Y family DNA polymerases may be relevant during translesion synthesis where changes in Mg^{2+} and Mn^{2+} concentrations under different cellular conditions could contribute to the regulation of Y family DNA polymerase activity during DNA replication.

REFERENCES

1. Fang, J. L., and Vaca, C. E. (1995) *Carcinogenesis* **16,** 2177–2185
2. Fang, J. L., and Vaca, C. E. (1997) *Carcinogenesis* **18,** 627–632
3. Matsuda, T., Terashima, I., Matsumoto, Y., Yabushita, H., Matsui, S., and Shibutani, S. (1999) *Biochemistry* **38,** 929–935
4. Baan, R., Straif, K., Grosse, Y., Secretan, B., El Ghissassi, F., Bavard, V., Altieri, A., and Cogliano, V. (2007) *Lancet Oncol.* **8,** 292–293
5. Seitz, H. K., and Becker, P. (2007) *Alcohol Res. Health* **30,** 38–47
6. Perrino, F. W., Blans, P., Harvey, S., Gelhaus, S. L., McGrath, C., Akman, S. A., Jenkins, G. S., Lacourse, W. R., and Fishbein, J. C. (2003) *Chem. Res. Toxicol.* **16,** 1616–1623
7. Upton, D. C., Wang, X., Blans, P., Perrino, F. W., Fishbein, J. C., and Akman, S. A. (2006) *Chem. Res. Toxicol.* **19,** 960–967
8. Franklin, M. C., Wang, J., and Steitz, T. A. (2001) *Cell* **105,** 657–667
9. Terashima, I., Matsuda, T., Fang, T. W., Suzuki, N., Kobayashi, J., Kohda, K., and Shibutani, S. (2001) *Biochemistry* **40,** 4106–4114
10. Upton, D. C., Wang, X., Blans, P., Perrino, F. W., Fishbein, J. C., and

[3] M. Pence and F. W. Perrino, unpublished data.

Akman, S. A. (2006) *Mutat. Res.* **599,** 1–10
11. Choi, J. Y., and Guengerich, F. P. (2006) *J. Biol. Chem.* **281,** 12315–12324
12. Choi, J. Y., and Guengerich, F. P. (2005) *J. Mol. Biol.* **352,** 72–90
13. Choi, J. Y., Angel, K. C., and Guengerich, F. P. (2006) *J. Biol. Chem.* **281,** 21062–21072
14. Prakash, S., Johnson, R. E., and Prakash, L. (2005) *Annu. Rev. Biochem.* **74,** 317–353
15. Nair, D. T., Johnson, R. E., Prakash, S., Prakash, L., and Aggarwal, A. K. (2004) *Nature* **430,** 377–380
16. Nair, D. T., Johnson, R. E., Prakash, L., Prakash, S., and Aggarwal, A. K. (2005) *Structure* **13,** 1569–1577
17. Nair, D. T., Johnson, R. E., Prakash, L., Prakash, S., and Aggarwal, A. K. (2006) *Structure* **14,** 749–755
18. Johnson, R. E., Washington, M. T., Haracska, L., Prakash, S., and Prakash, L. (2000) *Nature* **406,** 1015–1019
19. Johnson, R. E., Haracska, L., Prakash, L., and Prakash, S. (2006) *Mol. Cell. Biol.* **26,** 6435–6441
20. Perrino, F. W., Harvey, S., Blans, P., Gelhaus, S., Lacourse, W. R., and Fishbein, J. C. (2005) *Chem. Res. Toxicol.* **18,** 1451–1461
21. Nair, D. T., Johnson, R. E., Prakash, L., Prakash, S., and Aggarwal, A. K. (2006) *Nat. Struct. Mol. Biol.* **13,** 619–625
22. Beese, L. S., Friedman, J. M., and Steitz, T. A. (1993) *Biochemistry* **32,** 14095–14101
23. Beese, L. S., and Steitz, T. A. (1991) *EMBO J.* **10,** 25–33
24. Yang, W., Lee, J. Y., and Nowotny, M. (2006) *Mol. Cell* **22,** 5–13
25. Garcia-Diaz, M., Bebenek, K., Krahn, J. M., Pedersen, L. C., and Kunkel, T. A. (2007) *DNA Repair* (*Amst.*) **6,** 1333–1340
26. Sirover, M. A., and Loeb, L. A. (1976) *Science* **194,** 1434–1436
27. Sirover, M. A., and Loeb, L. A. (1976) *Proc. Natl. Acad. Sci. U. S. A.* **73,** 2331–2335
28. Frank, E. G., and Woodgate, R. (2007) *J. Biol. Chem.* **282,** 24689–24696
29. Boosalis, M. S., Petruska, J., and Goodman, M. F. (1987) *J. Biol. Chem.* **262,** 14689–14696
30. Pflugrath, J. W. (1999) *Acta Crystallogr. D Biol. Crystallogr.* **55,** 1718–1725
31. McCoy, A. J., Grosse-Kunstleve, R. W., Storoni, L. C., and Read, R. J. (2005) *Acta Crystallogr. D Biol. Crystallogr.* **61,** 458–464
32. Emsley, P., and Cowtan, K. (2004) *Acta Crystallogr. D Biol. Crystallogr.* **60,** 2126–2132
33. Winn, M. D., Murshudov, G. N., and Papiz, M. Z. (2003) *Methods Enzymol.* **374,** 300–321
34. Murshudov, G. N., Vagin, A. A., and Dodson, E. J. (1997) *Acta Crystallogr. D Biol. Crystallogr.* **53,** 240–255
35. Delano, W. L. (2002) *PyMol*, Delano Scientific, Palo Alto, CA
36. Tissier, A., McDonald, J. P., Frank, E. G., and Woodgate, R. (2000) *Genes Dev.* **14,** 1642–1650
37. Zhang, Y., Yuan, F., Wu, X., and Wang, Z. (2000) *Mol. Cell. Biol.* **20,** 7099–7108
38. Kunkel, T. A., and Loeb, L. A. (1979) *J. Biol. Chem.* **254,** 5718–5725
39. Rabkin, S. D., Moore, P. D., and Strauss, B. S. (1983) *Proc. Natl. Acad. Sci. U. S. A.* **80,** 1541–1545
40. Johnson, R. E., Prakash, L., and Prakash, S. (2005) *Proc. Natl. Acad. Sci. U. S. A.* **102,** 10466–10471
41. Washington, M. T., Minko, I. G., Johnson, R. E., Wolfle, W. T., Harris, T. M., Lloyd, R. S., Prakash, S., and Prakash, L. (2004) *Mol. Cell. Biol.* **24,** 5687–5693
42. Wolfle, W. T., Johnson, R. E., Minko, I. G., Lloyd, R. S., Prakash, S., and Prakash, L. (2005) *Mol. Cell. Biol.* **25,** 8748–8754
43. Wolfle, W. T., Johnson, R. E., Minko, I. G., Lloyd, R. S., Prakash, S., and Prakash, L. (2006) *Mol. Cell. Biol.* **26,** 381–386
44. Alt, A., Lammens, K., Chiocchini, C., Lammens, A., Pieck, J. C., Kuch, D., Hopfner, K. P., and Carell, T. (2007) *Science* **318,** 967–970
45. Lone, S., Townson, S. A., Uljon, S. N., Johnson, R. E., Brahma, A., Nair, D. T., Prakash, S., Prakash, L., and Aggarwal, A. K. (2007) *Mol. Cell* **25,** 601–614
46. Romani, A. (2007) *Arch. Biochem. Biophys.* **458,** 90–102
47. Kehres, D. G., and Maguire, M. E. (2003) *FEMS Microbiol. Rev.* **27,** 263–290
48. Kehres, D. G., Zaharik, M. L., Finlay, B. B., and Maguire, M. E. (2000) *Mol. Microbiol.* **36,** 1085–1100